Draft version December 5, 2008
Preprint typeset using LaTeX style emulateapj v. 10/09/06

LATE TIME OBSERVATIONS OF GRB 080319B: JET BREAK, HOST GALAXY AND ACCOMPANYING SUPERNOVA

N. R. Tanvir, E. Rol
Department of Physics and Astronomy, University of Leicester, University Road, Leicester, LE1 7RH, United Kingdom

A. J. Levan
Department of Physics, University of Warwick, Coventry, CV4 7AL, United Kingdom

A. S. Fruchter
Space Telescope Science Institute, 3700 San Martin Drive, Baltimore, MD 21218, USA

J. Granot
Centre for Astrophysics Research, University of Hertfordshire, College Lane, Hatfield, AL10 9AB, United Kingdom

K. M. Svensson
Department of Physics, University of Warwick, Coventry, CV4 7AL, United Kingdom

P. T. O'Brien, K. Wiersema, R. L. C. Starling
Department of Physics and Astronomy, University of Leicester, University Road, Leicester, LE1 7RH, United Kingdom

P. Jakobsson
Centre for Astrophysics and Cosmology, Science Institute, University of Iceland, Dunhagi 5, IS 107 Reykjavik, Iceland

J. Fynbo, J. Hjorth
Dark Cosmology Centre, Niels Bohr Institute, University of Copenhagen, Juliane Maries vej 30, 2100, Copenhagen, Denmark

P. A. Curran
Mullard Space Science Laboratory, Holmbury St. Mary, Dorking, RH5 6NT, United Kingdom

A. J. van der Horst, C. Kouveliotou
NASA/Marshall Space Flight Center, NSSTC, 320 Sparkman Drive, Huntsville, Alabama 35805, USA

J. L. Racusin, D. N. Burrows
Department of Astronomy and Astrophysics, 525 Davey Lab, Pennsylvania State University, University Park, PA, USA

and

F. Genet
Centre for Astrophysics Research, University of Hertfordshire, College Lane, Hatfield, AL10 9AB, United Kingdom

Draft version December 5, 2008

ABSTRACT

The *Swift* discovered GRB 080319B was by far the most distant source ever observed at naked eye brightness, reaching a peak magnitude of 5.3 at a redshift of $z = 0.937$. We present our late time optical and X-ray observations, which confirm that an achromatic break occurred in the power-law afterglow light curve at $\sim 10^6$ s post-burst. This most likely indicates that the gamma-ray burst (GRB) outflow was collimated, which for a uniform jet would imply a total energy in the jet $E_{\rm jet} \gtrsim 10^{52.5}$ erg. Our observations also show a late-time excess of red light, which is well explained if the GRB was accompanied by a supernova, similar to those seen in some other long-duration GRBs. The latest observations are dominated by light from the host and show that the GRB took place in a faint dwarf galaxy ($r(AB) \approx 27.2$, rest-frame $M_B \approx -17.3$). This galaxy is small even by the standards of other GRB hosts, which is suggestive of a low metallicity environment.

Subject headings: gamma rays: bursts - galaxies: high-redshift - supernovae: individual

Electronic address: nrt3@star.le.ac.uk

1. INTRODUCTION

GRB 080319B was one of the brightest gamma-ray bursts (GRBs) yet seen in gamma-rays, and uniquely bright in optical and X-ray wavelengths. At a redshift of $z = 0.937$ (Vreeswijk et al. 2008) this also translates to a record-breaking intrinsic peak luminosity in the optical, being approximately two magnitudes brighter than GRB 990123 (Akerlof et al. 1999) and a magnitude brighter than GRB 050904 (Haislip et al. 2006).

By good fortune, an earlier burst, GRB 080319A, had already taken place nearby on the sky roughly 25 minutes before GRB 080319B, so several wide-field optical cameras obtained imaging throughout the prompt phase, giving unprecedented coverage of the optical flash, and showing it to reach a visual magnitude 5.3 (Racusin et al. 2008).

Despite (or perhaps because of) the exceptionally dense multi-wavelength coverage of this event and its afterglow, modeling its properties has proven difficult. The extreme prompt behaviour is most naturally understood if the (soft) gamma-rays are dominated by synchrotron self-Compton (SSC), i.e. inverse-Compton up-scattering of (optical) synchrotron photons that are produced by the same population of relativistic electrons. If this is the case, then 2nd-order SSC should create another peak of emission in the GeV regime, of even greater total fluence (Kumar & Panaitescu 2008; Piran et al. 2008; Racusin et al. 2008). This potentially leads to a serious energy crisis, with the total radiated and kinetic energies, if isotropic, being comparable to or even in excess of the rest-mass energy of a massive star. It has long been thought that GRB outflows are likely to be collimated into narrow jets, and that this could reduce the total energy requirement by 1–3 (and in extreme cases perhaps more) orders of magnitude. The observational signature of such beaming is an achromatic break (hereafter referred to as a "jet-break") in the power-law decline of afterglow light (Rhoads 1999; Sari, Piran, & Halpern 1999). However, the luminosity of GRB 080319B and its afterglow may still stretch plausible models for both the prompt and afterglow emission.

Racusin et al. (2008) proposed a model in which the jet giving rise to the GRB has a particularly high-velocity, bright and narrow ($\sim 0.2^\circ$) core which produces a jet-break ~ 1 hour post burst, and dominates the early emission. A wider ($\sim 4^\circ$), more "conventional" jet surrounds this and dominates at intermediate and late times. This second jet is assumed to give rise to the break at $\sim 10^6$ seconds seen in the *Swift*/XRT light curve.

In a model of this sort, the extreme behaviour of the burst is partially explained by the low probability of an observer being within the aperture of the narrow jet. For GRB 080319B the fraction of observers viewing the gamma-ray emission from the bright and narrow jet would be roughly a factor of 400 lower than those seeing the broad jet. It also provides a reasonably good description of aspects of the temporal evolution of the afterglow. However, the model also requires a further coincidence of a (rarely seen) strong reverse shock from the wider jet creating the early optical afterglow, and this double coincidence seems a less natural scenario. We also note that such an extreme ratio of opening angles and solid angles between the wide and narrow jet components is much larger than the ratio of ~ 3 in opening angles expected in the original motivations for the two component jet models, which include the cocoon in the context of the collapsar model and the neutron decoupling during the acceleration and collimation of a hydromagnetic jet (see Peng, Königl & Granot 2005, and references therein). Furthermore, the required half-opening angle of the narrow jet (0.2°) is extremely small, and only slightly above the inverse of the initial Lorentz factor.

An alternative model developed by Racusin et al. (2008) has a single jet, ploughing into a complex density medium. In this case, the evolution of the cooling break frequency is proposed to drive the changes in the broad spectral-energy distribution (SED) of the afterglow.

Regardless of the successes and limitations of such models, it is clearly of great interest to investigate the late-time behavior of GRB 080319B and to place it in context with other bursts, which may provide independent clues to its nature. Is the late time evolution comparable to that seen in most long duration GRBs? In particular, is the sharp break in the X-ray lightcurve at $\sim 10^6$ seconds achromatic, as predicted for a jet break, and what does this imply for the energetics of the burst? Is the burst accompanied by a characteristic type Ic supernova (SN)? Is the underlying host galaxy similar to those of other long-duration GRBs?

In this paper we describe our late-time optical and X-ray monitoring of the transient and host galaxy emission of GRB 080319B, utilizing Gemini-North, *HST*, the VLT and *Chandra*.

2. OBSERVATIONS AND REDUCTION

2.1. *X-ray observations*

In order to follow the X-ray lightcurve out to late times, beyond the sensitivity limit of the Swift-XRT, we obtained observations with Chandra/ACIS (S3 chip), roughly 38 and 58 days after the burst. Total exposure times of 9 and 36 kiloseconds resulted in fluxes measured as $7.5^{+2.9}_{-2.4} \times 10^{-15}$ erg cm^{-2} s^{-1} and $4.0^{+1.1}_{-0.9} \times 10^{-15}$ erg cm^{-2} s^{-1} respectively. For the conversion from count rate to flux, we used the measured photon index and absorption for the late-time Swift data (assuming no spectral changes at these late times), since the number of counts in the Chandra data were too few for a spectral fit. We measured the count rates in the 0.3-7 keV energy range, which had relatively litte background noise, and converted these to 0.3-10 keV unabsorbed fluxes using WebPIMMS. The 1σ errors were derived using Bayesian confidence limit estimation (Kraft et al. 1991).

2.2. *Optical/nIR observations*

Due largely to its brightness, early optical and near-infrared (nIR) observations of GRB 080319B were pursued by several groups, resulting in a very well-sampled optical/nIR lightcurve covering the first few hours after the burst (Racusin et al. 2008; Bloom et al. 2008; Wozniak et al. 2008; Pandey et al. 2008). Despite its initial brightness the afterglow faded rapidly, and photometric monitoring required large aperture telescopes after a few days.

A log of all our late-time observations is provided in table 1. This does not include any correction for dust extinction: the foreground extinction is expected to be

small ($A_V = 0.037$, Schlegel et al. 1998) while the extinction internal to the host, although rather uncertain due to the presence of a break between the optical and X-ray, is also found to be modest (Racusin et al. 2008).

We obtained optical observations with Gemini-N/GMOS, VLT/FORS1 and *HST*/WFPC2, between ~ 3 and ~ 110 days post-burst. Processing of ground-based observations was performed using standard IRAF routines. In particular the GMOS reduction made use of the relevant customized software provided by Gemini. Photometric calibration, both zero-point and color terms, were obtained using SDSS stars in the field (Adelman-McCarthy et al. 2007; Cool et al. 2008). For consistency, the FORS1 B-band imaging was also calibrated to AB magnitudes.

For our *HST*/WFPC2 observations we placed the target on the WFALL aperture, on the corner of WFC3 closest to the apex, in order to reduce the impact of charge transfer inefficiency (CTE effect), which is significant for the old detectors operating on WFPC2. A 4-point dither pattern was used, and subexposures stacked using the DRIZZLE (Fruchter & Hook 2002) software onto a 0.05 arcsec pixel grid (from the native 0.1 arcsec pixels). Photometry of the transient was obtained in a 0.2 arcsec diameter aperture, and aperture corrections to the standard 1 arcsec diameter calculated using brighter point sources on the frame. CTE correction was performed using the method of Dolphin[1], although we applied only half the correction to the final epoch since the source is clearly extended[2] (extra allowance was made in the error budget for this step). The HST photometry was calibrated to AB magnitudes by reference to the tabulated zero points[3], and then transformed to SDSS r and i magnitudes for comparison with the ground-based data via the NICMOS Unit Conversion Form[4].

The position of the afterglow was determined, relative to two well positioned SDSS stars in the field to be: RA=14:31:40.994, dec=+36:18:08.64 (J2000), with an error of 0.02 arcsec in each coordinate.[5]

3. RESULTS

Our new X-ray and optical photometry is plotted in Figure 2, together with data from the literature. We expect the optical light curve to consist of three components: the afterglow of the GRB, any accompanying supernova and a steady underlying host galaxy. In the X-ray the emission is likely to be entirely from the afterglow.

In disentangling these components, our approach is to compare the photometry (corrected for the small foreground Galactic extinction) with a simple, self-consistent model of a power-law afterglow with a sharp achromatic break, and supernova. As we will show, this model matches the broad features of the data well, and allows us to focus on the main implications of the late-time observations, without getting embroiled in the fine details of the earlier time evolution. The parameters for the afterglow (adopting the convention flux $F \propto t^{-\alpha}\nu^{-\beta}$) are $\alpha_1 = 1.3$, characteristic of the pre-break decline, and $\alpha_2 = 2.35$ post-break. The break is taken to be abrupt and occur at 10^6 s, whilst the spectral slope through the optical bands is taken as $\beta = 0.5$ (Racusin et al. 2008). Finally, the supernova light curve is based on that of SN1998bw, consistent with what is found for several other GRB-SN (Galama et al. 2000; Zeh et al. 2004). We also include *in the model* a small amount of rest-frame extinction internal to the host of $A_V = 0.06$ (Wozniak et al. 2008), and assume a Pei (1992) SMC extinction law.

We expect the shorter wavelength observations (B and g-band) to be largely uncontaminated by supernova light, since SNe are weak rest-frame blue and UV emitters due to metal line blanketing. The redder bands therefore constrain any supernova component, which should rise to a peak roughly one month post burst. Finally our latest time observations are dominated by host galaxy emission. However, as shown below, even this late-time photometry is likely to be contaminated by some residual transient light. To allow for this we adopted an iterative procedure: first assuming the epochs at 100+ days show only host, using these magnitudes to correct the earlier photometry for host contribution, and thus allowing modeling of the transient emission. From this model we can then predict the remaining transient flux which is likely to still be in the latest observations, and hence we can re-estimate the host magnitudes with this contamination removed. The correction is about 30% in r and i and 10% in g, and we have increased the photometric error bars to allow that the contamination could actually range from zero up to this value. It is worth emphasizing that this correction has only a small effect on all but the 50+ day photometric points, and does not change the main conclusions we present.

3.1. *Jet-break and energetics*

Figure 2 (top panel) shows our late time *Chandra* observations, as well as early data taken by the *Swift*-XRT. Our X-ray observations confirm, and increase the confidence in, the break in the X-ray lightcurve at $t_b \approx 10^6$ seconds.

The photometry for the various optical bands, with host contribution subtracted (as described above; see also Section 3.3), are plotted in the lower panels of Figure 2. In the B and g-band observations, the light curve before and after the break is reasonably consistent with the X-ray slope and break time, indicating approximately achromatic behaviour, as expected for a jet break. In fact, this is one of the more convincing examples of a jet-break identified in the *Swift* era, when such clear achromatic behavior of X-ray and optical light curves has rarely been seen (Curran, van der Horst, & Wijers 2008).

Note that we are not concerned here with modelling the deviations from a simple power-law of the earlier time light-curves. This has already been considered in detail by Racusin et al. (2008) and Bloom et al. (2008). However, it is interesting to note that the sharpness of the late-time jet-break as seen in the X-rays is consistent with the optical observations, notably in the g-band. Such a sharp break is not expected for a wind-like external medium (Kumar & Panaitescu 2000), as considered

[1] http://purcell.as.arizona.edu/wfpc2_calib

[2] http://www.stsci.edu/hst/wfpc2/documents/isr/wfpc2_isr0004.html

[3] http://www.stsci.edu/documents/dhb/web/c32_wfpc2dataanal.fm1.html

[4] http://www.stsci.edu/hst/nicmos/tools/conversion_form.html

[5] Specifically the comparison stars used from SDSS release 6 were 587736943056454244 at RA=14:31:41.866, dec= +36:17:23.13 and 587736943056453784 at RA=14:31:42.912, dec= +36:18:24.26.

by Kumar & Panaitescu (2008), and so would require some modification to that simple model; for example, the coincidental presence of a wind-termination shock at around $R \sim 10^{18}$ cm could possibly be affecting the light curve at the same time as the jet-break.

If the break at $t_b \approx 10^6$ s is interpreted in the context of a simple model with a single jet (double sided, roughly uniform with reasonably sharp edges), it implies a half-opening angle of $\theta_j \sim 10^\circ$, for a canonical external medium density of $n \sim 1$ cm^{-3} and an (isotropic equivalent) kinetic energy comparable to that observed in gamma-rays, $E_{\rm k,iso} \sim E_{\gamma,\rm iso} = 1.4 \times 10^{54}$ erg (Sari, Piran, & Halpern 1999). This, in turn, implies a true energy output in gamma-rays within the observed energy range of $E_\gamma \sim 2 \times 10^{52}$ erg, and a comparable kinetic energy in the jet ($E_{\rm k} \sim E_\gamma$).

If the prompt optical and gamma-ray emission are due to synchrotron and synchrotron self-Compton (SSC), respectively, from the same emission region, then a second order SSC component is expected that carries $\gtrsim 10$ times more energy (Kumar & Panaitescu 2008; Racusin et al. 2008), i.e. $E_{\gamma,\rm SSC2} \gtrsim 10 E_\gamma$. In addition, a reasonable radiative efficiency of $\lesssim 20\%$ would suggest that the total initial energy is $E_{\rm jet} \gtrsim 5 E_{\gamma,\rm SSC2} \gtrsim 50 E_\gamma$, and is dominated by the kinetic energy that is left in the jet after the prompt emission. In this case, however, the implied jet half opening angle would be somewhat smaller, $\theta_j \sim 6^\circ$, implying $E_\gamma \sim 0.8 \times 10^{52}$ erg, $E_{\gamma,\rm SSC2} \gtrsim 8 \times 10^{52}$ erg and $E_{\rm jet} \gtrsim 4 \times 10^{53}$ erg.

Alternatively, the kinetic energy can also be estimated from the X-ray luminosity at 12 hr in the rest frame (Granot, Königl, & Piran 2006; Nousek et al. 2006), from which we find $E_{\rm k,iso} \approx 7 \times 10^{52}$ erg, for typical microphysical parameters ($\epsilon_e = 0.1$, $\epsilon_B = 0.01$, $p = 2.2$). This would in turn imply $\theta_{j,w} \sim 12^\circ$ and a true kinetic energy of $E_{\rm k,w} \sim 2 \times 10^{51}$ erg. The isotropic equivalent kinetic energy at this level would require a very high efficiency of the gamma-ray emission ($\gtrsim 95\%$) for a single wide jet, unless the microphysical parameters were very different so that $E_{\rm k,iso}$ would be significantly higher. If, on the other hand, the gamma-rays were produced by a narrow jet with a considerably higher $E_{\rm k,iso}$ then this can bring down the efficiency requirements to more reasonable values (Peng, Königl & Granot 2005). In fact, this feature is built into the two component jet model of Racusin et al. (2008), which postulates a very narrow ($\theta_{j,n} \sim 0.2^\circ$), very high Lorentz factor ($\Gamma \sim 10^3$) central jet, producing an early break in the light curve, coupled with a wider ($\theta_{j,w} \sim 4^\circ$) jet leading to the later time break we see at 10^6 s. This model also mitigates the energy crisis more effectively, with each jet producing $E_\gamma \approx 2 \times 10^{50}$ erg.

3.2. *The supernova*

The r, i and z-band observations (Figure 2 lower panels) do not show a break at the same time, but rather show at first a slowing optical decay, and marked reddening, followed by a steepening again after about 30 days. We interpret this as being due to the contribution to the optical light of an underlying supernova coming to dominate the afterglow in these bands. Such supernova "humps" have been seen in the light curves of several long-duration GRBs which have been monitored sufficiently deeply at late times (eg. Galama et al. 2000; Zeh et al. 2004).

As stated above, we follow the conventional procedure of assuming a light curve for the supernova component based on that of SN1998bw, which accompanied the low-redshift GRB 980425 (Galama et al. 1998). We redshifted and k-corrected these light curves to produce templates in our observed wavebands appropriate to $z = 0.937$, and faded these by 0.4 mag, consistent with the typical GRB-SN "humps" found by Zeh et al. (2004).

When added to the broken power-law afterglow, this produces quite a reasonable match to the photometry of the transient. Thus we find that GRB 080319B was accompanied by a supernova a little fainter than the prototype SN1998bw: whilst an even better match to the photometry would have been achieved with a model made either somewhat redder, or with the peak time a little earlier (a stretch factor < 1 in the language of Zeh et al. 2004). This is in slight disagreement with Bloom et al. (2008) who, using more preliminary and less complete set of late-time photometry, concluded that a supernova component rather brighter than SN1998bw was required.

3.3. *The host galaxy*

Our second epoch HST observations revealed that the afterglow, while still detected, was clearly superimposed upon faint, extended host galaxy emission, with the transient slightly offset north by about 0.2 arcsec from the centre of this emission (Levan et al. 2008). By the third epoch the galaxy clearly dominates and is revealed to be a very faint, low surface brightness source extending over roughly 0.5 arcsec. It is not well detected in the WFPC2 images, so the photometry carries a large uncertainty. As described above, we attempt to remove the residual transient light by subtracting the flux predicted by our simple model. Hence we find (foreground extinction corrected) host magnitudes of $r(AB) = 27.20 \pm 0.44$ and $i(AB) = 25.86 \pm 0.26$, and from the last Gemini-N/GMOS g-band image, $g(AB) = 26.80 \pm 0.14$.

This final photometry, while limited, does allow for a crude fit to the galaxy SED. In particular the relatively blue g-r color (-0.46 ± 0.46), coupled with the red $r - i$ (1.4 ± 0.5), is suggestive of a moderately strong Balmer break, implying the presence of an older stellar population, in addition to the young population which produces the blue rest-frame UV color, and presumably seeded the GRB.

In Figure 3 we show these photometric points fitted with a star-forming galaxy template with the following properties: $M_V = -17.5 \pm 0.2$, $M_B = -17.3 \pm 0.2$ (quoted errors are statistical: systematic errors arising from uncertainties in the template library and fitting procedures may be two or three times this), implying stellar mass $M = 8.2 \times 10^7 M_\odot$ and star formation rate $= 1.4 M_\odot$ year^{-1}. The best fit has an internal extinction $A_V = 0$, which although poorly constrained by our limited photometry, is consistent with the low extinction seen to the afterglow. This luminosity corresponds to about $0.02 L_*$ at the observed redshift (Willmer et al. 2006). Such a small galaxy is likely to have low metallicity, although quantifying this is hard, not least because of the small number of data points available for the fit and their large photometric uncertainties. Based on the

$z \sim 0.7$ mass-metallicity relationship of Savaglio et al. (2005), the implied metallicity is $12 + \log(O/H) = 7.8$, or about 1/7 solar. However, this numerical value should be treated with caution for various reasons: firstly, the absolute calibration of the mass-metallicity relation is difficult, and we note that Savaglio et al. (2008) using a revised calibration based on Kewley & Ellison (2008) found metallicities to decrease by ~ 0.5 dex; and secondly, in the same paper Savaglio et al. (2008) show that GRB hosts with spectroscopically estimated metallicities scatter quite widely around this relation in any case.

These properties are within the range of other GRB host galaxies (e.g. Fruchter et al. 2006; Savaglio et al. 2008), but at the very faint end of this sample. The location of the galaxy in the redshift – magnitude plane is shown in Figure 4, which shows that it is by some way the faintest yet observed by HST at comparable redshift. Similarly, the model fit would imply a specific star formation rate at the high end and stellar mass at the low end, compared to a sample of other GRB hosts (Figure 5). We caution that a proportion of these redshifts were obtained from host rather than afterglow spectroscopy, and hence there is some bias against very faint hosts. For illustration, these are shown in a separate panel on the right side of Figure 4. A particular case in point is that of GRB 980326 which also exhibited a "supernova hump" in its light curve suggestive of a redshift $z \sim 1$, but had a host galaxy with $R > 27$ (Bloom et al. 1999).

Finally, we note that the final Chandra X-ray point is somewhat above the power-law extrapolation of the earlier light curve. It is conceivable that this is due to X-ray flux from the host itself becoming significant (the final point corresponds to a luminosity 1.8×10^{43} erg s^{-1}), however, this would require a very high star formation rate (Watson et al. 2004) or AGN component, both of which are rare amongst GRB hosts (Tanvir et al. 2004). Rather more likely is that this is an instance of "overshooting" of the afterglow light curve, where the initial post-break decline is steeper than its long-term assymptotic decay rate due to the limb-brightening of the (unresolved) afterglow image (Granot 2007).

4. SUMMARY

We have presented a late time optical and X-ray lightcurve for the exceptionally bright GRB 080319B. These data allow us to decompose the contributions from afterglow, supernova and underlying host galaxy. We find that the afterglow of GRB 080319B exhibited an achromatic break in its lightcurve at $\approx 10^6$ seconds, which can be interpreted as being due to the relativistic outflow being initially confined within a jet. If uniform, the total energy of the jet is given by $E_{\rm jet} \gtrsim 3.8 \times 10^{52} \times (n/1\,{\rm cm}^{-3})^{1/4} (E_{\gamma,{\rm iso}}/1.4 \times 10^{54}\,{\rm erg})^{3/4}$ erg. Thus, for $E_{\gamma,{\rm iso}} \sim 1 \times 10^{55}$ erg, if 2nd-order synchrotron self-compton photons dominate the radiation energy budget, we have $E_{\rm jet} \gtrsim 2 \times 10^{53}$ erg. For more complex jet structures in which the gamma-ray and late afterglow arise from different components, such as the two component jet model of Racusin et al. (2008), the total jet energy can be smaller.

In addition GRB 080319B was associated with a bright supernova, slightly fainter in luminosity than the prototype SN1998bw. Such supernovae, inferred from red "humps" in their light curves, have been inferred to accompany several other GRBs at similar redshifts (e.g. Zeh et al. 2004), and indeed GRB 080319B represents one of the best examples.

Finally, we have detected a faint host galaxy under the position of the GRB, which is smaller than other GRB hosts observed so far at comparable redshifts. This is likely to indicate a low-metallicity environment, and one might speculate that this could be related to the extreme properties of the burst. However it is also notable that most of the weakest GRBs known (particularly GRB 980425 and GRB 060218) have also have occurred in small, low-metallicity hosts and been accompanied by energetic type Ibc supernovae.

We acknowledge useful discussions with Daniele Malesani and Ralph Wijers.

We are grateful to Matt Mountain for awarding directors discretionary time on HST to observe GRB 080319B under program GO/DD 11513 (PI: Tanvir). Based on observations made with the NASA/ESA Hubble Space Telescope, obtained at the Space Telescope Science Institute, which is operated by the Association of Universities for Research in Astronomy, Inc., under NASA contract NAS 5-26555.

Based on observations obtained at the Gemini Observatory, which is operated by the Association of Universities for Research in Astronomy, Inc., under a cooperative agreement with the NSF on behalf of the Gemini partnership: the National Science Foundation (United States), the Science and Technology Facilities Council (United Kingdom), the National Research Council (Canada), CONICYT (Chile), the Australian Research Council (Australia), Ministrio da Cincia e Tecnologia (Brazil) and SECYT (Argentina)

This publication has made use of data obtained with the Chandra X-ray Observatory, under program ID 09500789. (observations IDs 9134 and 9135)

Based on observations made with ESO Telescopes at the La Silla or Paranal Observatories under programme ID 081.D-0853

The DARK Cosmology Centre is funded by the Danish National Research Foundation.

We particularly thank the staff of the VLT and Gemini for their efforts in obtaining the optical data, and those at CXC for their assistance in scheduling the Chandra observations. We also gratefully acknowledge the work of the wider *Swift* team that makes this research possible. NRT, ER and AJL are supported by STFC. JG gratefully acknowledges a Royal Society Wolfson Research Merit Award.

Facilities: HST (WFPC2), CXO (ACIS), Gemini-North(GMOS), VLT(FORS1).

REFERENCES

Adelman-McCarthy, J. K., et al. 2007, ApJS, 172, 634
Akerlof, C., et al. 1999, Nature, 398, 400
Bloom J. S., et al., 1999, Nature, 401, 453
Bloom, J. S., et al. 2008, ApJ submitted, arXiv:0803.3215
Bruzual A., G., & Charlot, S. 2003, MNRAS, 344, 1000
Cool, R. J., et al. 2008, GRB Coordinates Network, 7465,
Cram, L., Hopkins, A., Mobasher, B., & Rowan-Robinson, M. 1998, ApJ, 507, 155

Curran P. A., van der Horst A. J., Wijers R. A. M. J., 2008, MNRAS, 386, 859
Fruchter, A. S., & Hook, R. N. 2002, PASP, 114, 144
Fruchter, A. S., et al. 2006, Nature, 441, 463
Galama, T. J., et al. 1998, Nature, 395, 670
Galama, T. J., et al. 2000, ApJ, 536, 185
Granot J., Königl A., Piran T., 2006, MNRAS, 370, 1946
Granot, J. 2007, Revista Mexicana de Astronomia y Astrofisica, vol. 27, 27, 140
Haislip, J. B., et al. 2006, Nature, 440, 181
Kewley, L. J., & Ellison, S. L. 2008, ApJ, 681, 1183
Kraft, R. P., Burrows, D. N., & Nousek, J. A. 1991, ApJ, 374, 344
Kumar, P., & Panaitescu, A. 2000, ApJ, 541, L51
Kumar, P., & Panaitescu, A. 2008, MNRAS, 391, L19
Levan, A. J., Tanvir, N. R., & Fruchter, A. S. 2008, GRB Coordinates Network, 7710, 1
Mannucci, F., Della Valle, M., Panagia, N., Cappellaro, E., Cresci, G., Maiolino, R., Petrosian, A., & Turatto, M. 2005, A&A, 433, 807
Nousek, J. A., et al., 2006, ApJ, 642, 389
Pandey, S. B., et al., 2008, A&A, submitted
Pei, Y. C. 1992, ApJ, 395, 130
Peng, F., Königl, A., & Granot, J. 2005, ApJ, 626, 966
Piran, T., Sari, R., & Zou, Y.-C. 2008, arXiv:0807.3954
Racusin, J. L., et al. 2008, Nature, 455, 183
Rhoads, J. E. 1999, ApJ, 525, 737
Sari R., Piran T., Halpern J. P., 1999, ApJ, 519, L17
Savaglio, S., et al. 2005, ApJ, 635, 260
Savaglio, S., Glazebrook, K., & Le Borgne, D. 2008, ApJ in press, arXiv:0803.2718
Schlegel, D. J., Finkbeiner, D. P., & Davis, M. 1998, ApJ, 500, 525
Tanvir, N. R., et al. 2004, MNRAS, 352, 1073
Tanvir, N. R., Levan, A. J., Fruchter, A. S., Graham, J., Wiersema, K., & Rol, E. 2008a, GRB Coordinates Network, 7569
Tanvir, N. R., Perley, D. A., Levan, A. J., Bloom, J. S., Fruchter, A. S., & Rol, E. 2008b, GRB Coordinates Network, 7621
Vreeswijk, P., et al. 2008, GRB Coordinates Network, 7444
Watson, D., Hjorth, J., Jakobsson, P., Pedersen, K., Patel, S., & Kouveliotou, C. 2004, A&A, 425, L33
Willmer C. N. A., et al., 2006, ApJ, 647, 853
Wozniak P. R., Vestrand W. T., Panaitescu A. D., Wren J. A., Davis H. R., White R. R., ApJin press, arXiv:0810.2481
Zeh, A., Klose, S., & Hartmann, D. H. 2004, ApJ, 609, 952

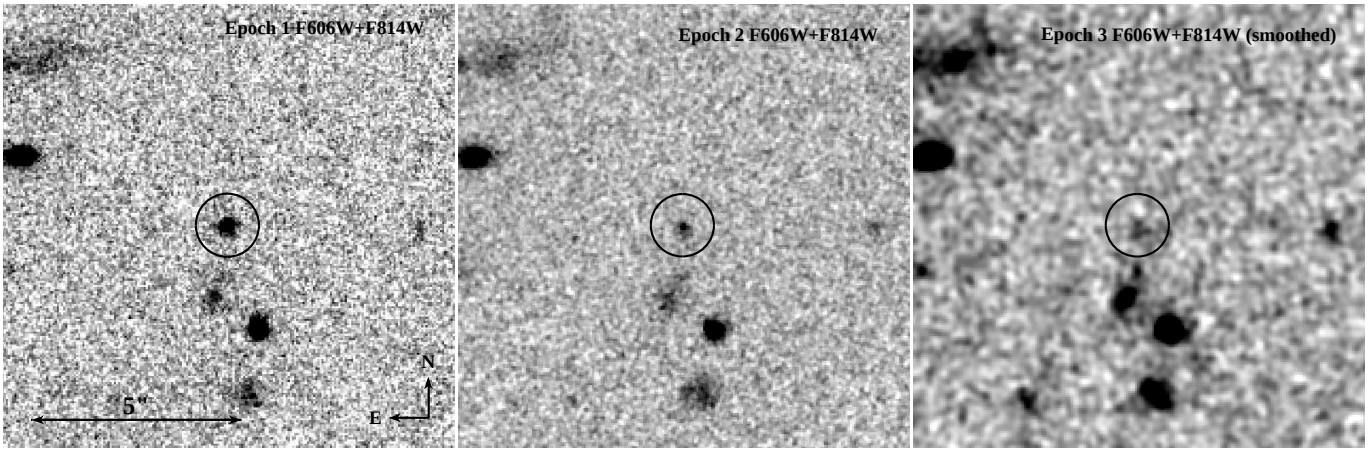

FIG. 1.— Images (F606W and F814W combined) at each epoch, as labelled. The phases are afterglow, supernova and host dominated respectively. Note that the final panel has been smoothed with a gaussian kernel to bring out the faint host galaxy light.

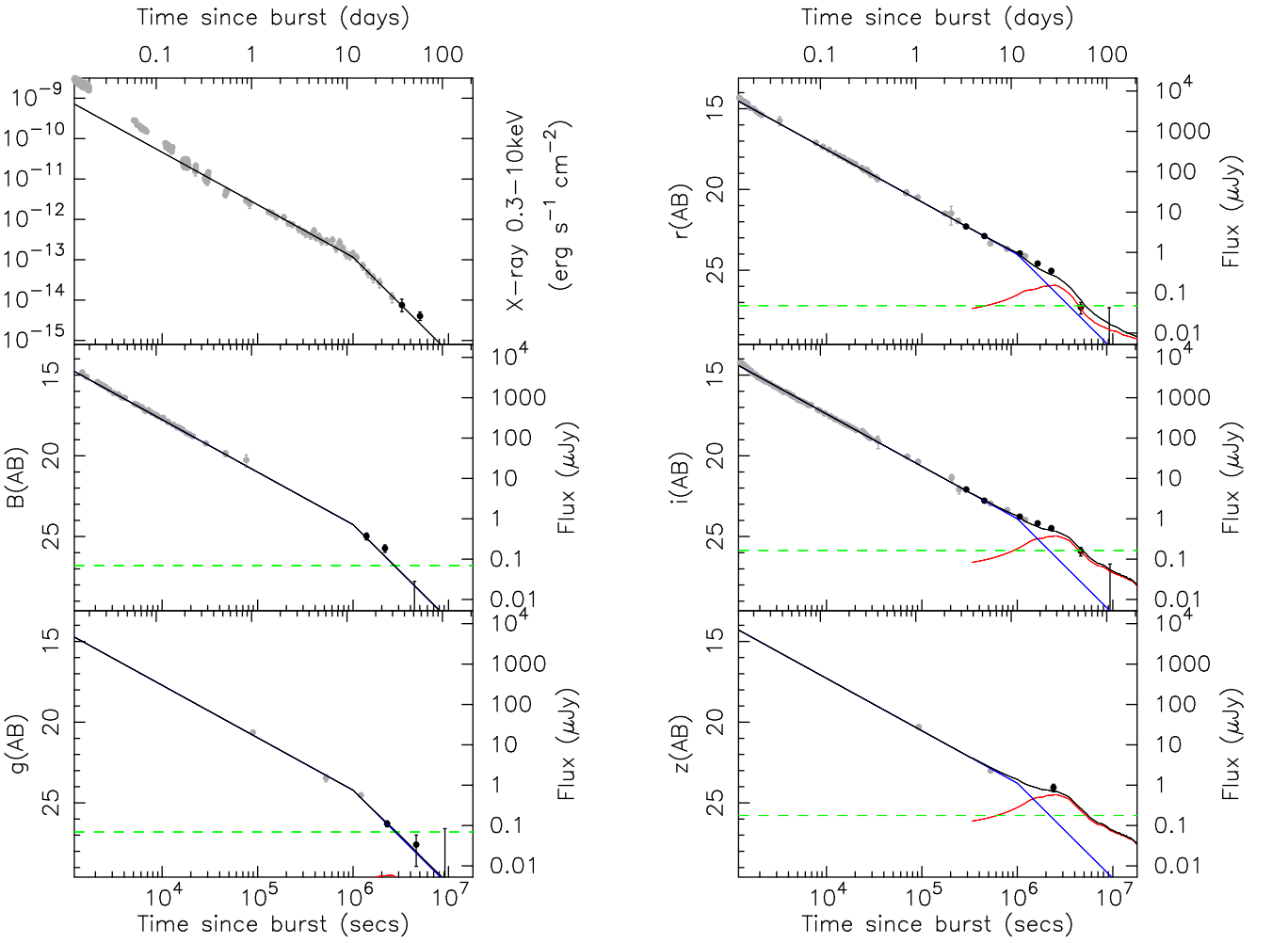

FIG. 2.— Late time photometry of GRB 080319B, with bold symbols indicating observations reported here, and light symbols being data-points from the literature (Bloom et al. 2008; Racusin et al. 2008, and references therein). Photometry has been corrected for foreground extinction, and error bars are 1σ. The green dashed lines are the estimated magnitudes of the host galaxy which have been subtracted from the ground-based data. In the case of HST images the point source photometry is done on a scale smaller than the host. The blue line is the model afterglow, and the red line the model supernova light curve, as described in the text. The black line is their sum.

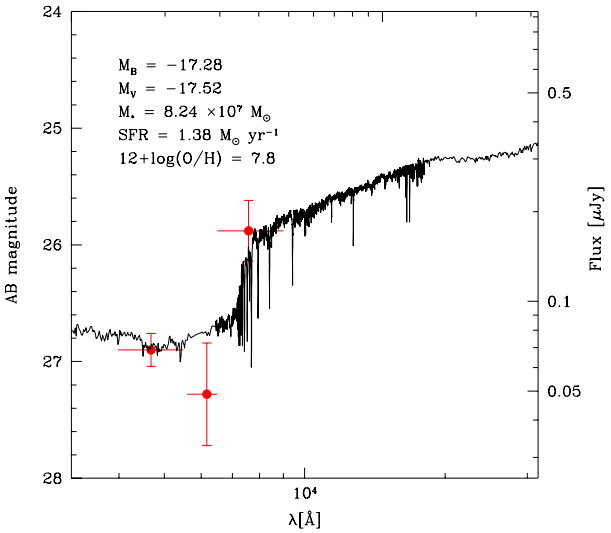

FIG. 3.— A model spectrum fitted to the three host photometry points. The best fit model is a young star forming galaxy (Bruzual & Charlot 2003). Physical parameters are derived from the restframe SED: star formation rates (SFRs) are derived from the U-band luminosity (Cram et al. 1998); stellar mass is estimated from the K-band luminosity with a color correction to the mass-to-light ratio (Mannucci et al. 2005). The χ^2_ν of the fit is relatively poor, ~ 2.1, mainly due to a suppression in the r-band which is not well fit by any model, albeit that the data point itself is consistent at the $\sim 1\sigma$ level.

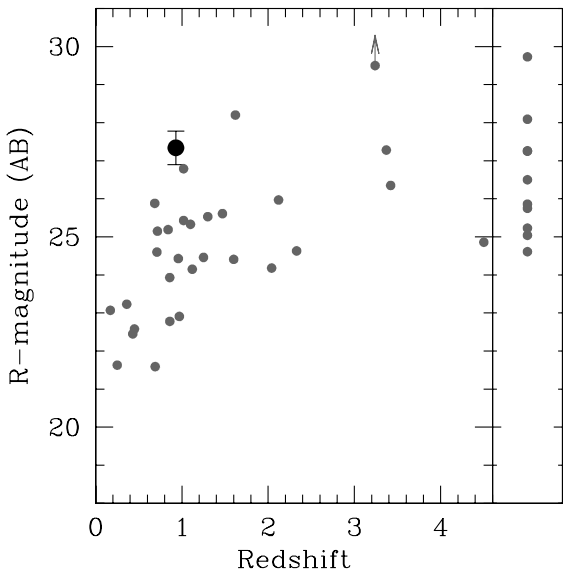

FIG. 4.— The R(AB) magnitude of the host of GRB 080319B compared to a sample of other GRB hosts observed by HST as a function of redshift. Those without redshifts are shown in the right hand column. Clearly the GRB 080319B host is faint, even by the standards of other GRB hosts.

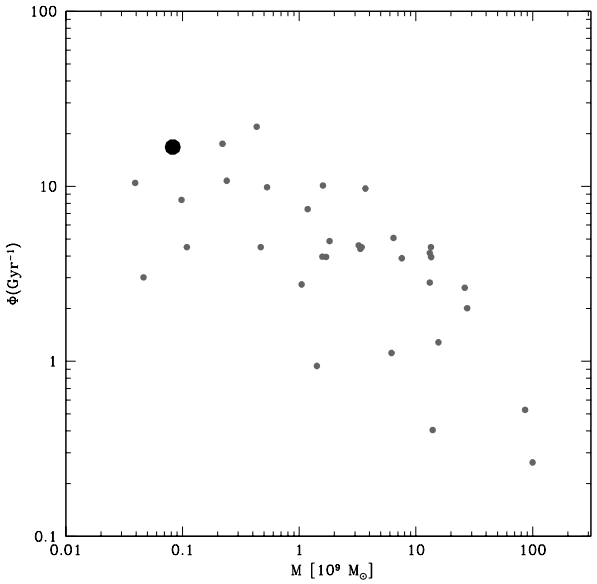

FIG. 5.— Plot of specific star formation rate versus stellar mass for a sample of GRB hosts. The host of GRB 080319B, indicated by a large, bold symbol, is at the extreme low mass and high specific star formation rate end of the distribution. The host galaxy sample is that used by Svensson et al. (in prep), and includes all GRB hosts with $z < 1.2$ and any photometric detections (as reported by http://www.grbhosts.org/ an references therein). Parameters determined by SED fits to the photometry, as detailed in the caption to Fig. 3.

TABLE 1
Log of late-time observations reported here. This photometry is not corrected for extinction, but the small aperture HST photometry has been aperture and CTE corrected as described in the text.

Time post-burst (days)	Telescope/ camera	Filter	Exposure time (s)	Flux (μJy)	Error	Aperture (diameter arcsec)
3.36	Gemini-N/GMOS	r	5×200	4.33	0.08	2.0
3.38	Gemini-N/GMOS	i	5×200	5.40	0.10	2.0
5.22	Gemini-N/GMOS	r	5×100	2.51	0.09	2.0
5.23	Gemini-N/GMOS	i	5×100	2.91	0.11	2.0
12.3	Gemini-N/GMOS	r	5×100	0.96	0.05	2.0
12.3	Gemini-N/GMOS	i	5×100	1.27	0.07	2.0
26.3[a]	Gemini-N/GMOS	g	6×180	0.174	0.013	1.5
26.3[a]	Gemini-N/GMOS	r	6×180	0.39	0.03	1.5
26.3[a]	Gemini-N/GMOS	i	6×180	0.74	0.03	1.5
27.7[a]	Gemini-N/GMOS	z	6×180	1.09	0.16	1.5
53.2	Gemini-N/GMOS	g	9×300	0.099	0.020	1.5
106.1	Gemini-N/GMOS	g	9×350	0.072	0.007	1.5
16.0	VLT/FORS1	B	6×300	0.49	0.08	1.5
25.0	VLT/FORS1	B	6×300	0.24	0.04	1.5
51.0	VLT/FORS2	B	18×300	0.071	0.023	1.5
18.9[b]	HST/WFPC2	F606W	8×400	0.55	0.01	0.2
19.1[b]	HST/WFPC2	F814W	8×400	0.81	0.02	0.2
53.4[c]	HST/WFPC2	F814W	8×400	0.200	0.023	0.2
53.6[c]	HST/WFPC2	F606W	8×400	0.066	0.006	0.2
106.4	HST/WFPC2	F606W	8×400	0.033	0.009	0.2
				0.065	0.028	1.0
108.3	HST/WFPC2	F814W	8×400	0.046	0.027	0.2
				0.219	0.045	1.0